The 2014 World Congress on
Advances in Civil, Environmental, and Materials Research (ACEM14)
Busan, Korea, August 24-28, 2014

Structural Improvement Analysis of Working Rail Mounted Cranes under Wind Loads

*Hui Jin[1)], Da Chen[2)]

[1), 2)] *Jiangsu Key Laboratory of Engineering Mechanics & Key Laboratory of Concrete and Prestressed Concrete Structures of Ministy of Education, Southeast University, Nanjing, 210096, China*
[1)] jinhui@seu.edu.cn

ABSTRACT

The external devices or electromechanical systems are not effective enough to prevent frequent wind accidents of rail mounted cranes. Taking the 300 ton shipbuilding gantry crane as the research object, this paper aims to improve cranes' self-structures to promote their windproof abilities fundamentally. The total wind force applied on the crane was calculated by the design rules to evaluate the correctness of the wind field. And based on the analysis of the bearing force state in properly sized field by FLUENT, two highest-pressure areas could be found on the windward side of the crane. To decrease the high-pressure areas, six different structural improvement schemes were proposed, and the most effective one could be determined according to the maximized deduction of the wind force. Finally, the dynamic simulation by ADAMS revealed the impressive decreasing amplitude of braking time and distance of improved cranes, verifying the effectiveness of the structural improvement.

1. INTRODUCTION

Currently, different kinds of rail mounted cranes are utilised in the field work, including the 300 ton shipbuilding gantry crane, one of the most popular large-scale mechanical equipment. This kind of crane is composed of three parts, as shown in Figs. 1(a)-(b). The flexible leg bears small wind force with little windward area. While the girder and rigid leg have larger windward areas, leading to threatening wind loads, which can easily overturn the crane due to its large mass and high barycenter position. The wind accident happens frequently, especially when the crane works in open areas

---

[1)] Associate Professor

[2)] Graduate Student

Hui Jin and Da Chen contributed equally to this work and should be considered co-first authors.

such as ports, where typhoons or sudden wind gusts are quite common (Simiu 1986，Forristall 1988，Ochi 1988，Mara 2010，Han 2011， McCarthy 2009).

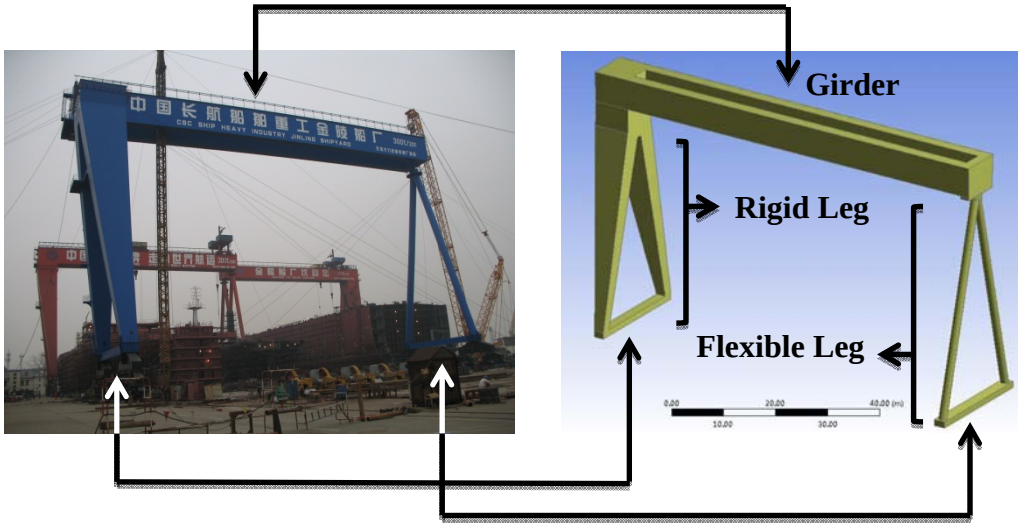

(a) (b)

Fig.1 300 ton shipbuilding gantry crane

Not just the 300 ton shipbuilding gantry crane, almost all kinds of rail mounted cranes are suffering from the wind accidents. To prevent such accidents and ensure the working safety, standards and scholars recommend differents methods and devices to enhance the windproof abilities of cranes. The crane design specifications suggested to use the crane wheel brake to supply continuous braking torque (Zhang 2001). McCarthy proposed a ductile link tie-down system to improve the dockside crane's hurricane resistance and reliability (McCarthy 2009). Bao presented various static and dynamic measures, which are popular in the practical engineering application (Bao 2006). Nearly all criterions and articles are focusing on the external devices or electromechanical systems. However, they are not effective enough in most cases (Wu 2011).

To solve the above problem, this paper concentrates on the self-structures of cranes and investigates the structural improvement to bring down the wind load fundamentally. Section 2 calculates the wind force according to the design rules and analyses the wind field of 300 ton shipbuilding gantry crane, in order to present the high-pressure areas. Section 3 compares six different structural improvement schemes to determine the best one. And Scetion 4 simulates the change of braking time and distance between improved and unimproved cranes to highlight the structural improvement. Finally, this paper is concluded in Section 5.

2. ANLYSIS OF THE WIND FIELD

2.1 Wind force according to the design rules for cranes

Analysis of the bearing force state of the working 300 ton shipbuilding gantry crane under wind loads provides the theoretical basis for the structural improvement. The total wind force calculated by the design rules for cranes (GB/T3811-2008) is used as a benchmark to ensure the correctness and precision of the wind field in Section 2.2, which is vital to the analysis of the bearing force state and pressure distribution on the crane.

According to the design rules for cranes, the wind load applied on cranes can be obtained as

$$F=CPA(\sin\theta)^2 \tag{1}$$

in which

$$P=0.625v^2 \tag{2}$$

$$A=\frac{1-\eta^N}{1-\eta}\varphi A' \tag{3}$$

where C is the wind force coefficient (1.8252 for the girder, 1.6768 for the rigid leg and 0.7 for the flexible leg), P is the wind pressure, A is the area of windward side, θ is the angle between the wind direction and the structure surface (81° for the rigid leg and 76.537° for the flexible leg), v is the wind velocity, η is the reduction factor (0.1 for the girder and 0.81344 for the flexible leg), N = 2 is the number of components, φ = 1 is the windward filling percentage of the first structure, A' is the area of the first windward structure. All above coefficients are calculated by the standard design drawings of the 300 ton shipbuilding gantry crane.

Typical wind velocities of wind scales are used in Eq. (1) to obtain the detailed wind force applied on the crane, as shown in Table .1.

Table.1 Detailed wind force according to the design rules for cranes

Wind scale	Wind velocity (m/s)	Wind force (kN)			
		Girder	Rigid leg	Flexible leg	Total
4	8.25	45.61	13.91	4.01	63.54
6	19.95	266.72	81.35	23.46	371.54
8	28.35	538.62	164.28	47.38	750.28
9	33.15	736.45	224.62	64.78	1025.86
10	38.4	988.19	301.40	86.93	1376.52
12	48.9	1602.48	488.77	140.97	2232.22
13	58.95	2328.86	710.32	204.87	3244.05

2.2 Simulation of the wind field

The wind force calculated by design rules is only estimated and general value, which

cannot present the precise bearing force state of cranes. Simulation of the wind field is a perfect solution, and is able to indicate the direction of the structural improvement

A full-size model of the 300 ton shipbuilding gantry crane is developed in FLUENT module of the software ANSYS, as shown in Fig. 1(b). The wheels and cars are ignored, which have little influence on the wind force and may lead to calculation failures. Specific size of cuboid wind field is determined, ensuring the total force applied on crane is approximately equal to the criterion value in Table 1 (see Fig. 2(a)-(d)). The difference of wind force between these two methods is less than 4%, which is detailed in Table. 2.

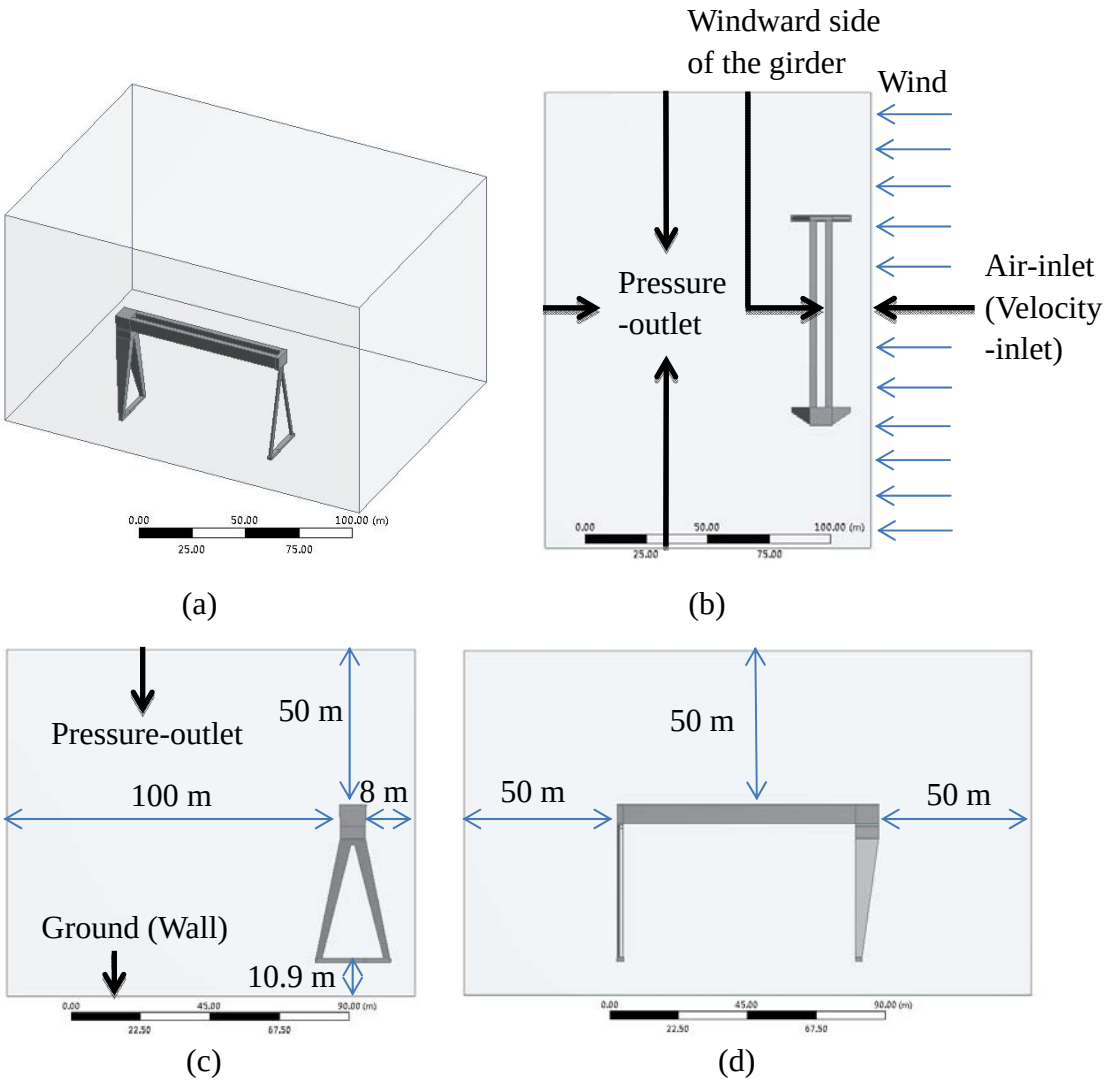

Fig.2 Model of the wind field

As shown in Figs. 2(b)-(c), all six surfaces of the field are set as different boundary conditions. The air-inlet surface is set as velocity-inlet, which hypothesizes that all wind

applied on this surface is of the same and constant speed. The ground is set as wall without air transmission. And the other four surfaces are defined as pressure-outlet with zero gauge pressure. The hydraulic diameter and turbulent intensity included in the boundary conditions are calculated by Eqs. (4)-(5), respectively. Above settings ensure that this model is able to cope with backflow on the exit and can reach the convergence precision.

$$D_H=4\frac{A_o}{\chi} \tag{4}$$

and

$$I=0.16\left(\frac{\rho V D_H}{\mu}\right)^{-0.125} \tag{5}$$

where D_H is the hydraulic diameter, A_o is the effective cross section area, and χ is the wetted perimeter, I is the turbulent intensity, ρ is the air density (1.225kg /m^3), V is the wind velocity, D_H is the hydraulic diameter calculated by Eq. (4), and μ is the air viscosity (1.7894×10^{-5} $P_a\cdot S$).

The field model is meshed by Hex Dominant method, with hexahedrons on the surface and tetrahedrons in the internal. The elements enclosing the crane are refined to obtain an accurate result (see Fig. 3).

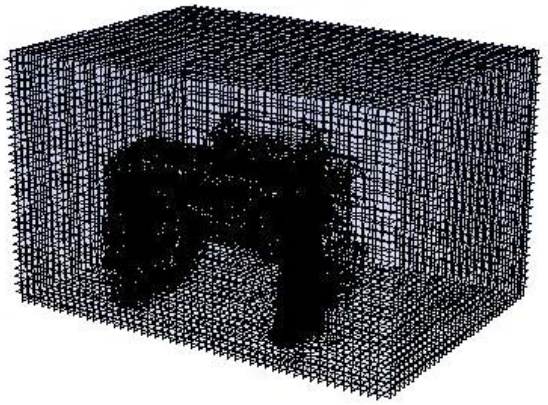

Fig.3 Elements of the wind field

The wind field is a typical turbulent flow field and the calculation model is defined as standard k-ε model, which aims for fully developed turbulence and is most widely used in engineering calculations. The turbulence kinetic energy k and its rate of dissipation ε are determined by following transport equations (Wang 2004, Wang 1994, Ansys help):

$$\frac{\partial}{\partial t}(\rho k)+\frac{\partial}{\partial x_i}(\rho k u_i)=\frac{\partial}{\partial x_j}\left[\left(\mu+\frac{\mu_t}{\sigma_k}\right)\frac{\partial k}{\partial x_j}\right]+G_k+G_b-\rho\varepsilon-Y_M+S_k \tag{6}$$

and

$$\frac{\partial}{\partial t}(\rho\varepsilon)+\frac{\partial}{\partial x_i}(pku_i)=\frac{\partial}{\partial x_j}\left[\left(\mu+\frac{\mu_t}{\sigma_\varepsilon}\right)\frac{\partial\varepsilon}{\partial x_j}\right]+C_{1\varepsilon}\frac{\varepsilon}{k}(G_k+C_{3\varepsilon}G_b)-C_{2\varepsilon}\rho\frac{\varepsilon^2}{k}+S_\varepsilon \quad (7)$$

where G_k is the generation of turbulence kinetic energy due to the mean velocity gradients, G_b represents the generation of turbulence kinetic energy due to buoyancy, Y_M is the contribution of the fluctuating dilatation in compressible turbulence to the overall dissipation rate, and $C_{1\varepsilon}$, $C_{2\varepsilon}$, $C_{3\varepsilon}$ are constants, σ_k and σ_ε represents the turbulent Prandtl numbers for k and ε, respectively. The other parameters are calculation coefficients or user-defined source terms.

According to the calculation by FLUENT based on the above settings, the bearing force state of the crane can be presented by the pressure distribution in the following figures, as well as the streamlines of the wind field. As displayed in Fig. 4, two highest-pressure areas exist on the windward side of the crane, concentrating on the junction between the girder and rigid leg (A in Fig. 4) and the flexible-leg side of the girder (B in Fig. 4). The lee side of the crane and internal side of the girder are covered with low-pressure areas. And whirlpools caused by high differential pressure emerge at the lee side of both highest-pressure areas (see Figs. 5(a)-(b)). The comparison of total wind force calculated by FLUENT and design rules is shown in Table 2, which demonstrates the correctness and precision of the simulation due to the little residuals (Hu 2012).

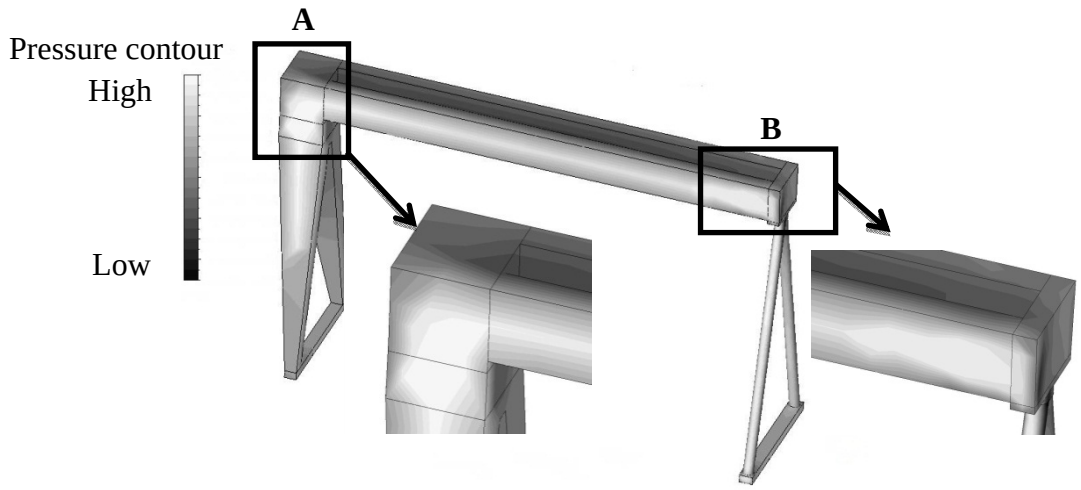

Fig.4 Pressure distribution on the crane

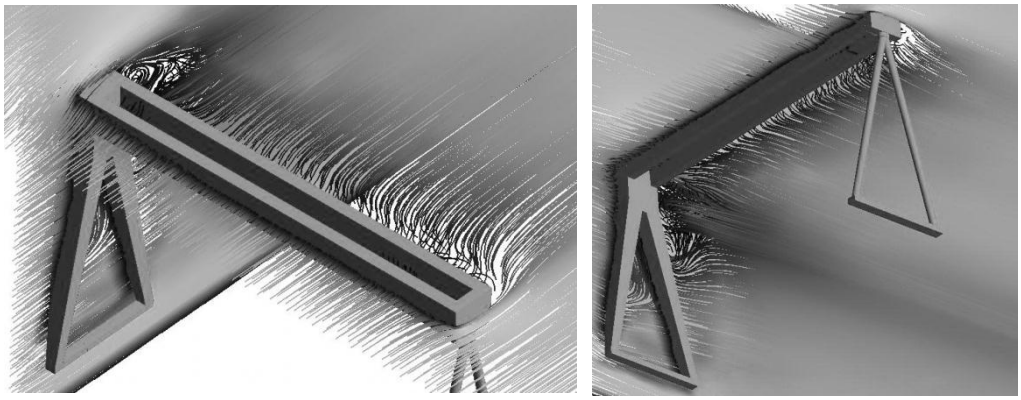

(a) (b)

Fig.5 Streamlines of the wind field

Table.2 Total wind force calculated by FLUENT and design rules

Wind scale	Wind velocity (m/s)	Wind force (kN)		Residual (%)
		FLUENT	Design rules	
4	8.25	65.16	63.54	2.55
6	19.95	385.099	371.54	3.65
8	28.35	752.064	750.28	0.238
9	33.15	1024.85	1025.86	0.098
10	38.40	1373.41	1376.52	0.226
12	48.9	2217.29	2232.22	0.67
13	58.95	3211.55	3244.05	1.00

3. ANALYSIS OF STRUCTUAL IMPROVEMENT

The wind force applied on the girder, rigid leg and flexible leg can be calculated by modelling and simulating them separately in the specific field. Accounting for about 54% of the total wind force, the load on the girder is the largest, while 36% is on the rigid leg, and only 10% acts on the flexible leg, indicating that most of the wind load is applied on the girder and rigid leg, which can also be certified by the pressure distribution shown in Fig. 4. Therefore, the key to improve the windproof performance of the crane is to minish the wind force on the girder and rigid leg, especially on the highest-pressure areas (A and B in Fig. 4).

Based on the above discussion, this paper investigates and simulates different structural improvement schemes focused on the deduction of high-pressure areas, of which pressure distributions are shown in Figs. 6(a)-(f), using the same wind field in the

previous section with correctness and precision already been proved.

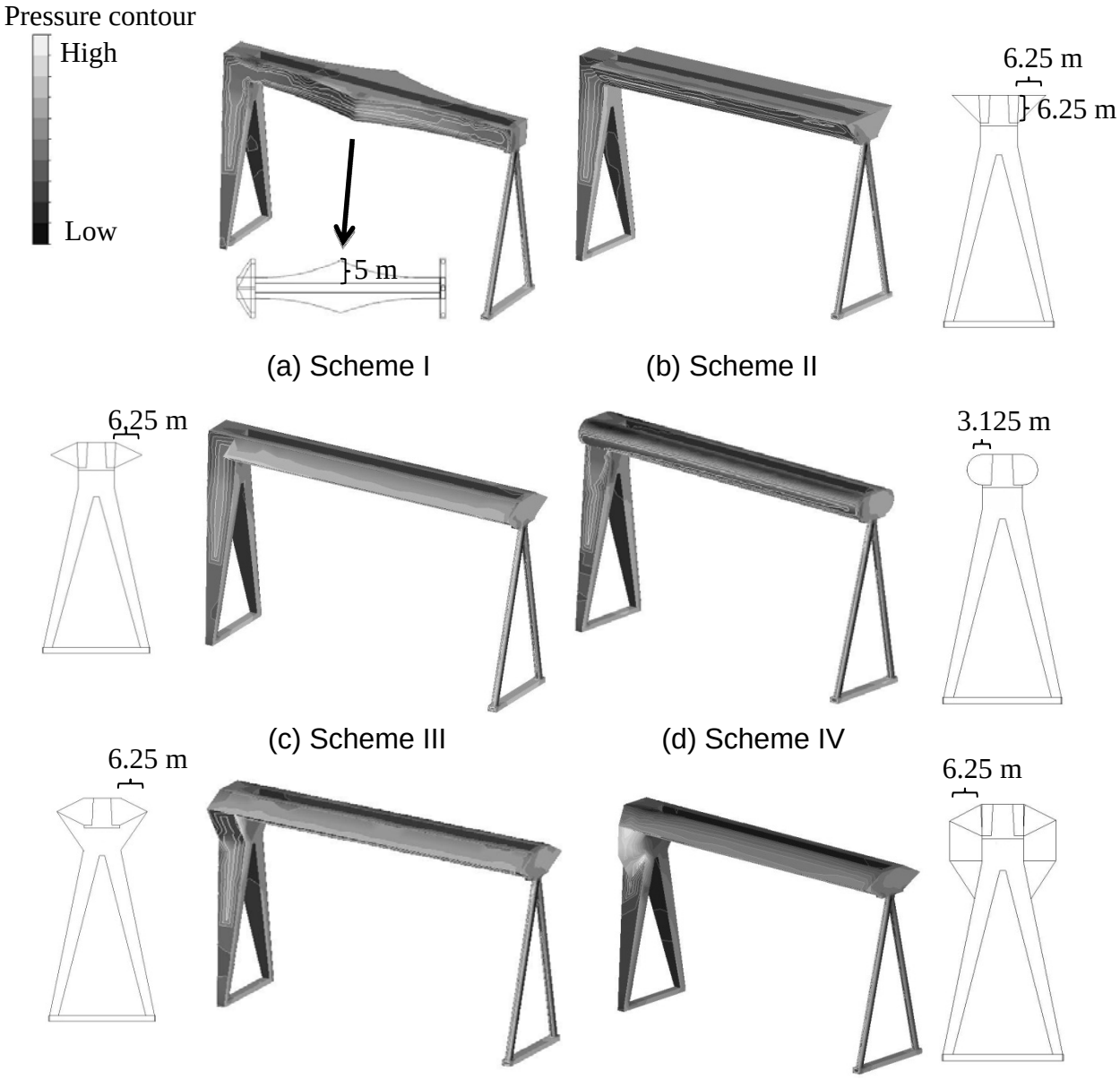

Fig.6 Pressure distributions of structural improvement schemes

The above first four schemes focus on the structural improvement of the girder. And the last two schemes integrate the improvements of both girder and rigid leg. To be specific, Scheme I changes the outline of the girder into the wave shape (see Fig. 6(a)), leading to not decrease but increase of the wind force. Scheme II also fails to minish the wind load, which promotes the cross section of the girder (see Fig. 6(b)). While when altering the cross section into another triangle shape, Scheme III successfully brings down the wind load (about 20%), as shown in Fig. 6(c). And Scheme IV tries the

semicircle section (see Fig. 6(d)), which has no better improvement effects (about 10%) than Scheme III. To sum up, Scheme III is capable of decreasing the wind force on the girder maximumly. Scheme V and Scheme VI incorporate Scheme III with different improvements of the rigid leg (see Figs. 6(e)-(f)), which give rise to varying effects (approximately 20% force deduction for Scheme V and 25% for Scheme VI), indicating that Scheme VI is the best structural windproof improvement method of the 300 ton shipbuilding gantry crane.

The following Fig. 7 presents detailed pressure distributions on the crane in Scheme VI, in which the previous high-pressure areas in Fig. 4 have disappeared. And with little whirlpools, the streamline distribution in Figs. 8(a)-(b) is much more smooth than the original one (see Figs. 5(a)-(b)). The comparison between wind force applied on the improved (Scheme VI) and unimproved structure is illustrated in Fig. 9, of which the average decreasing amplitude is 25.6%. All the analysis above demonstrates that the windproof ability of 300 ton shipbuilding gantry crane in scheme VI has been significantly improved (Chen 2012).

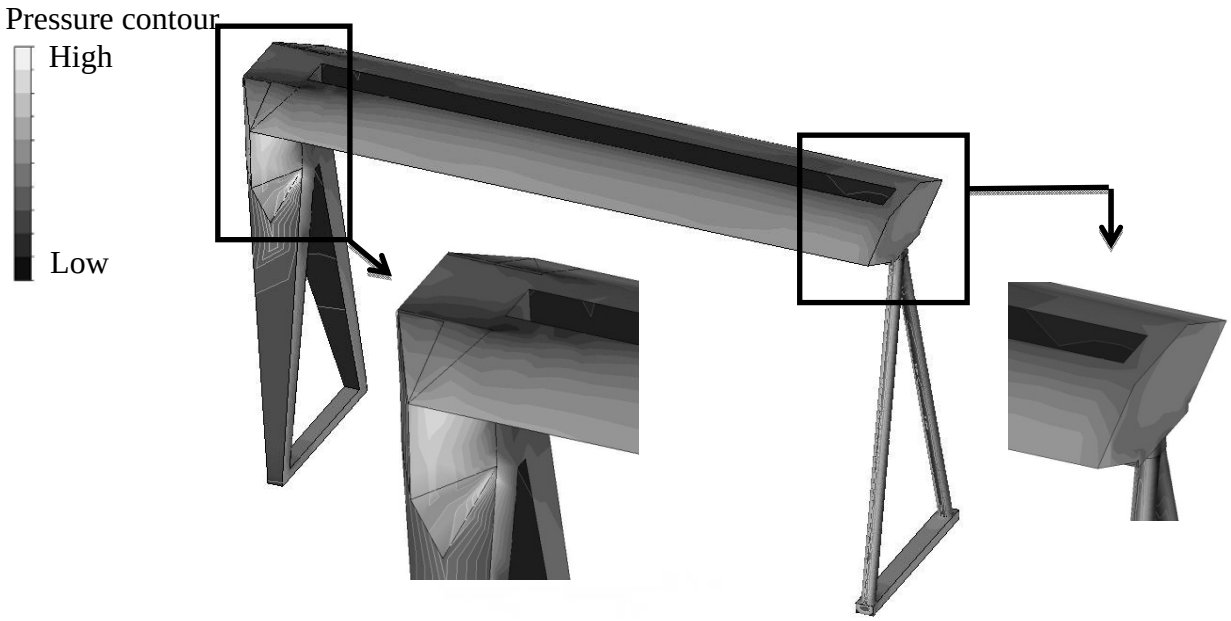

Figure.7 Pressure distribution on the crane in Scheme VI

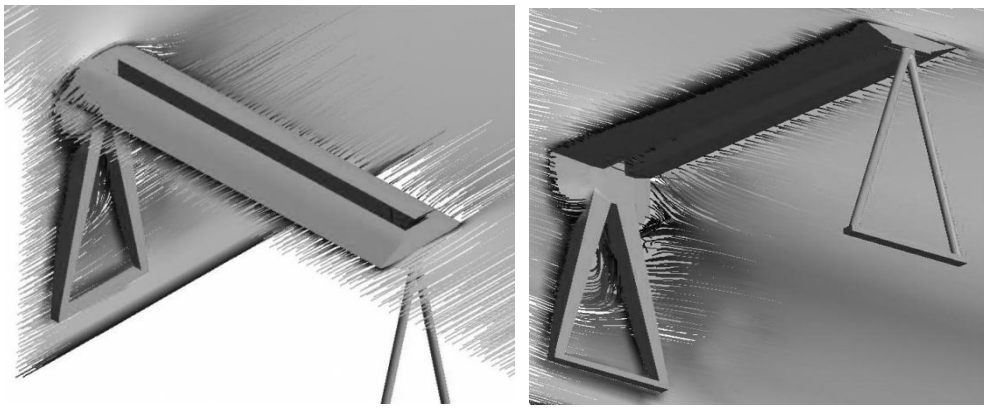

(a) (b)

Figure.8 Streamlines of the wind field in Scheme VI

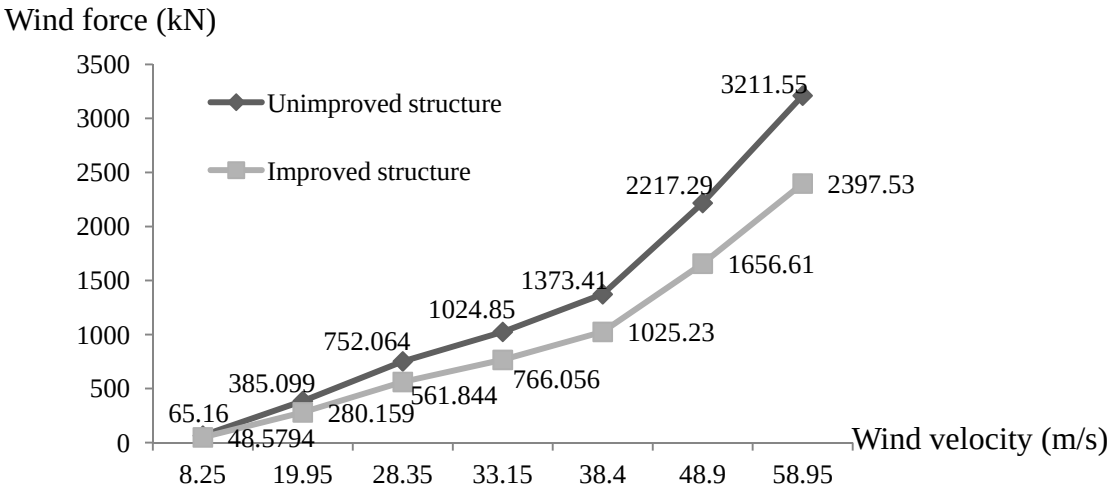

Fig.9 Comparison of the wind force

Considering the value of practicability and popularization, the improvement in Scheme VI allows transport cars moving in the middle of the girder, resulting in no influence on the daily work of the crane. Furthermore, with additional structures installed on the surface, which can be made of lightweight materials, the original load bearing structure and mechanical response will stay the same, ensuring the security and feasibility of this windproof improvement scheme in the practical application.

4. APPLICATION OF STRUCTUAL IMPROVEMENT

4.1 Dynamic numerical simulation

The improved (Scheme VI) and unimproved structures of the 300 ton shipbuilding gantry crane are modeled in the software ADAMS to investigate the change of dynamic performance. Both models ignore the internal structural response and simplistically

construct the crane as a rigid superstructure connected with wheels, as shown in Figs. 10(a)-(b).

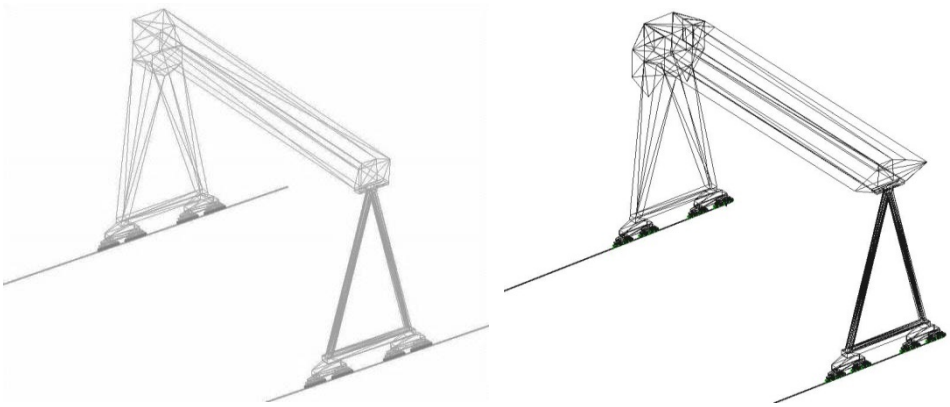

(a) Unimproved crane (b) Improved crane

Fig.10 Models of the 300 ton shipbuilding gantry crane

The travelling mechanism is crucial to the authenticity of this simulation. According to the practical situation, 64 rigid wheels are installed on each model with 32 brake wheels intervally arranged (see Fig. 11). Integrated with the whole superstructure by Boolean operation, the wheel axles are associated with wheels by revolution joints. And braking torque is applied on revolution joints of the brake wheels, as shown in Fig. 12. Simultaneously, moment of rolling resistance couple exists on every revolution joint of the free wheels and brake wheels.

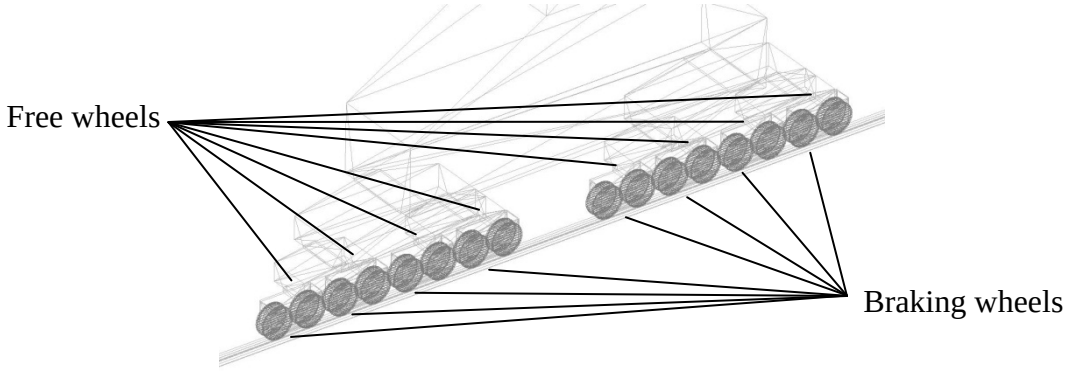

Figure.11 Crane wheels

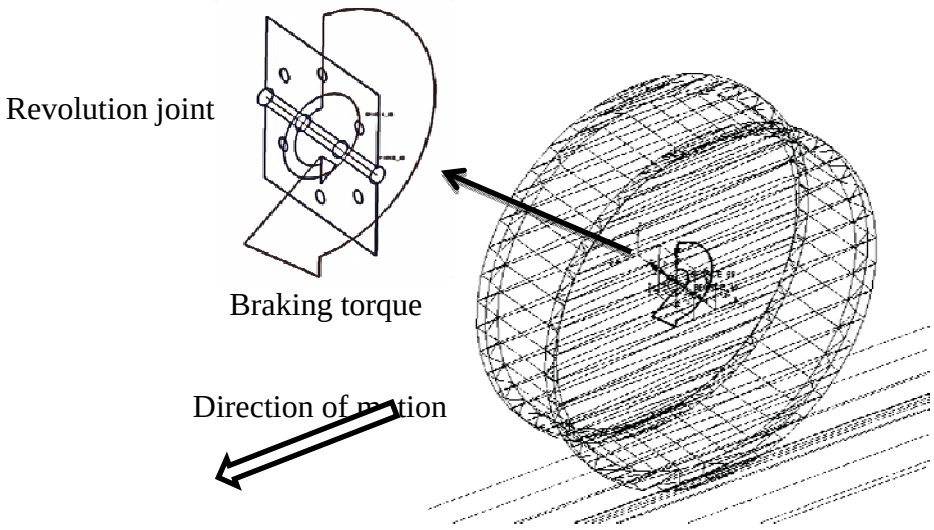

Fig.12 Brake wheel

The wind force is considered as a constant concentrated force applied on the barycenter of the crane body. And the improved crane is assumed to keep the same weight as the original one. The interaction between railway tracks and wheels is achieved by Coulomb contact force, which can be described as the following IMPACT function (Fan 2006, Yu 2006).

$$IMPAC = \begin{cases} Max(0,\ k(x_1 - x)^e - STEP(x, x_1 - d, c_{max}, x_1, 0) \cdot \dot{x} & x < x_1 \\ 0 & x \geq x_1 \end{cases} \tag{8}$$

where x is a distance variable used to compute the *IMPACT* function, x_1 is the free length of x, k is the stiffness of the boundary surface interaction, e is the exponent of the force deformation characteristic, c_{max} means the maximum damping coefficient, d is the boundary penetration at which ADAMS/Solver (C++) applies full damping, and *STEP* approximates a step function with a cubic polynomial determined by following Eq. (9).

$$STEP(x, x_0, h_0, x_1, h_1) = \begin{cases} h_0 & x \leq x_0 \\ h_0 + (h_1 - h_0)[(x - x_0)/(x_1 - x_0)]^2\{3 - 2[(x - x_0)/(x_1 - x_0)]\} & x_0 < x < x_1 \\ h_1 & x \geq x_1 \end{cases} \tag{9}$$

The models above are employed to investigate the distinction between different braking performance of improved and unimproved 300 ton shipbuilding gantry cranes under various working conditions, including different delay time (time between the application of wind force and the effectuation of braking torque), initial velocities, and wind loads, etc. The simulation results reveal the promotion of dynamic performance of the crane due to the structural improvement.

4.2 Results and discussion

Considering the constant braking torque (10 kN·m) and the same delay time (1 s) and initial velocity (0.6 m/s), curves of velocity and distance versus time (see Figs. 13(a)-(b) and Figs. 14(a)-(b)) can be obtained from the dynamic simulation of improved and unimproved cranes, under the 8 wind scale (28.5 m/s wind velocity) which applys 561.844 kN and 752.064 kN wind force on these two structures, respectively.

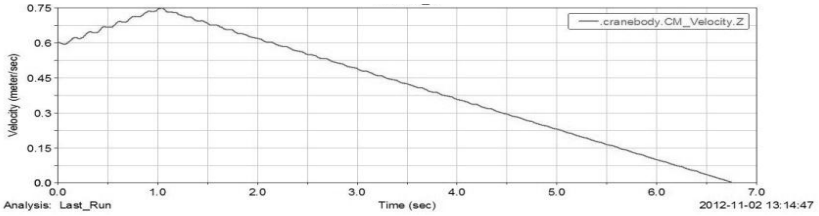

(a) Curve of velocity

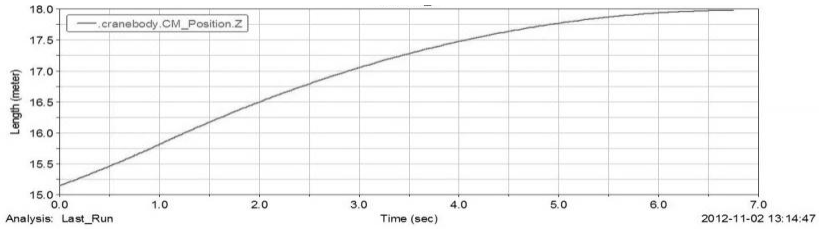

(b) Curve of distance

Fig.13 Curves of velocity and distance versus time of the improved crane

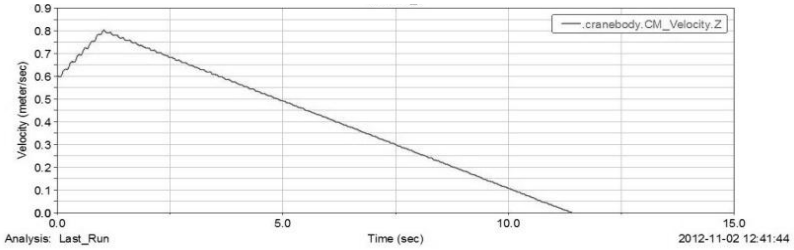

(a) Curve of velocity

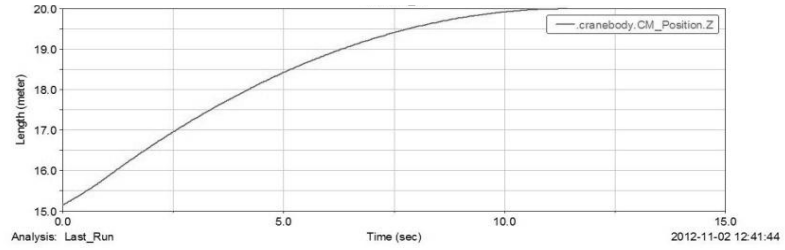

(b) Curve of distance

Fig.14 Curves of velocity and distance versus time of the unimproved crane

As shown in the Fig. 13(a) and Fig. 14(a), the braking time of the improved crane (6.75 s) is much less that the time of unimproved crane (11.40 s). And as displayed in the Fig. 13(b) and Fig. 14(b), the braking distance of the improved crane (2.8272 m) is also sharply less than the one of the unimproved crane (4.8469 m). With more than 40% of the decreasing amplitudes in both braking time and distance, the structural improvement can surely promote the braking ability and raise the dynamic safety of the crane. And vibrations can be found in the progress of crane's motion, on account of the vibrations of contact force and torque between the wheels and tracks.

Changing the working conditions (i.e. delay time, initial velocity and wind scale) presents a comprehensive comparison between the braking performance of improved and unimproved cranes, as shown in the following Table.3 (Jin 2013). Decreasing amplitudes in both braking time and distance of the improved crane remain almost the same, regardless of the variation of delay time and initial velocity. While the wind scale is the only factor which can influence the decreasing amplitude. The higher is the wind scale, the more the braking time and distance will decrease, indicating that the structural improvement will play an increasingly important role with the accelerated wind.

Table.3 Decreasing amplitude under different working conditions

	Unimproved crane		Improved crane		Decreasing amplitude	
	Braking Time(s)	Distance (m)	Braking Time(s)	Distance (m)	T (%)	S (%)
Delay time (s)	Initial velocity 0.6 m/s, wind scale 8					
0	7.6	2.2943	4.5	1.371	**40.79**	**40.24**
1	11.4	4.8469	6.75	2.8272	**40.79**	**41.67**
2	15.1	8.1784	8.95	4.6294	**40.73**	**43.39**
3	18.8	12.2762	11.15	6.769	**40.69**	**45.59**
Initial velocity (m/s)	Delay time 1 s, wind scale 8					
0.45	9.45	3.3059	5.6	1.9121	**40.74**	**42.16**
0.6	11.4	4.8469	6.75	2.8272	**40.79**	**41.67**
0.75	13.3	6.6736	7.9	3.9137	**40.6**	**41.36**
Wind scale	Initial velocity 0.6 m/s, delay time 1 s					
4	3.2837	1.2985	3.2	1.2737	**2.55**	**1.91**
6	4.9	2.0152	4.2	1.7132	**14.29**	**14.99**
8	11.4	4.8469	6.75	2.8272	**40.79**	**41.67**

Different braking torque will also lead to a disparity. The smaller is the braking torque, the larger is the decreasing amplitude, which can be combined with the above conclusions to prove that the structural improvement will ensure the safety of the crane especially under dangerous conditions (high wind scale and small braking torque).

The simulation of rail mounted cranes with different travelling mechanisms is conducted as well. All wheels are assumed to be the braking wheels with the same braking torque (5 kN·m). And result analysis reveals the analogous distinction between the braking performance of improved and unimproved cranes, which will not be described in this paper to avoid repetition.

5. CONCLUSIONS

The wind field of 300 ton shipbuilding gantry crane is developed to investigate the best structural improvement to bring down the wind force. And the dynamic simulation of improved and unimproved cranes confirms the effectiveness of the structural improvement. Conclusions from this study are summarized as follows:

(1) Two highest-pressure areas exist on the windward side of the crane, concentrating on the flexible-leg side of the girder and the junction between the girder and rigid leg, both accounting for a high percentage of the total wind force.

(2) The best structural improvement (see Fig. 6(f), Scheme VI) can decrease the wind force with a considerable amplitude, and eliminate the high-pressure areas.

(3) The structural improvement can tremendously promote the braking performance of the crane and keep its safety especially under dangerous conditions.

ACKNOWLEDGMENTS

The research was supported by the Natural Science Foundation of Jiangsu Province (BK2011613), the Science and Technology Project of General Administration of Quality Supervision, Inspection and Quarantine of the People′s Republic of China (2009QK153，2009QK149), Jiangsu Province Science and Technology Support Project (BE2012125), and A Project Funded by the Priority Academic Program Development of Jiangsu Higher Education Institutions.

REFERENCES

Simiu, E. and Scanlan, R.H. (1986), Wind Effects on Structures, Wiley & Son Inc, Houston, USA.

Forristall, G.Z. (1988), Wind Spectra and Gust Factors over Water, OTC 5735, Houston, USA.

Ochi, M.K. and Shin,Y.S. (1988), Wind Turbulent Spectra for Design Consideration of Offshore Structures, OTC 5735, Houston, USA.

Mara, T.G. and Asce, A.M. (2010), “Effects of a construction tower crane on the wind loading of a high-rise building”, Structural Engineering, 136(11), 1453-1460.

Han, D.S. and Han, G.J. (2011), “The difference in the uplift force at each support point of a container crane between FSI analysis and a wind tunnel test”, Mechanical Science and Technology, 25(2)(2011), 301-308.

McCarthy, P., Soderberg, E., and Dix, A. (2009), “Wind damage to dockside cranes: recent failures and recommendations”, Proceedings of Technical Council on Lifeline Earthquake Engineering Conference (TCLEE) 2009, Oakland, California, United States, June.

Zhang, Z.W., Yu, H.Q., Wang, J.N. and Bao, Q.F. (2001), Crane Design Manual, (2nd Edition), China Railway Publishing House, Beijing, China.

Bao, Q.F., Sheng, F. (2006), “Safe measures against wind disaster for large harbor cranes”, Hoisting and conveying machinery, 2006(11), 1-5.

Wu, X.L. (2011), “Dynamic analysis and application of wind-proof for working rail mounted crane”, MSE. Dissertation, Southeast University, Nanjing, China.

GB/T3811-2008, China crane design code (2008), Chinese standards press, Beijing, China.

Wang, F.J. (2004), Principle and Application of CFD software, Tsinghua University Press, Beijing, China.

Wang, J.P. (1994), “Computational fluid dynamics and engineering application”, Journal of Electrical Equipment, Vol. 5.

Ansys Help.

Hu, J.B., Chen, D., Ding, S.Q., Qing, G.W., Jin, H. (2012), “Simulation of the wind field of gantry cranes based on FLUENT”, Applied Mechanics and Materials, 217-219 (2012), 1530-1534.

Chen, D., Jin, H. (2012), “Simulation of the Wind Field of Gantry Cranes and Windproof Improvement of Structure”, Proceeding of The 1st International Conference on Structural Health Monitoring and Integrity Management, Beijing, China, November.

Fan, J.C., Xiong, G.M. and Zhou, M.F. (2006), Application and Improvement of Virtual Prototype Software MSC.ADAMS, China Machine Press, Beijing, China.

Yu, D.Y. and Qian, Y.J. (2006), “Parameter - settings for the dynamic simulation based on ADAMS”, Computer Simulation, 23(9), 103-183.

Jin, H., Chen, D. (2013), “Braking performance of working rail mounted cranes under wind load”, Wind and Structures (accepted).